JCI insight

Sensitive and adaptable pharmacological control of CAR T cells through extracellular receptor dimerization

Wai-Hang Leung, … , Jordan Jarjour, Alexander Astrakhan

JCI Insight. 2019;4(11):e124430. https://doi.org/10.1172/jci.insight.124430.

Research Article | Oncology | Therapeutics

Graphical abstract

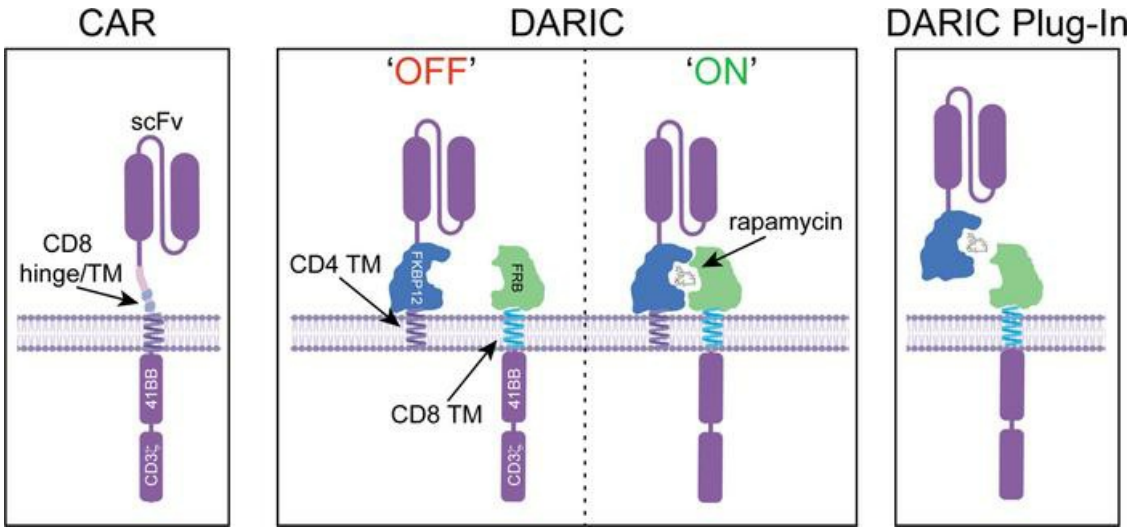

JCI insight

RESEARCH ARTICLE

Sensitive and adaptable pharmacological control of CAR T cells through extracellular receptor dimerization

Wai-Hang Leung,[1] Joel Gay,[1] Unja Martin,[1] Tracy E. Garrett,[1] Holly M. Horton,[1] Michael T. Certo,[1] Bruce R. Blazar,[2] Richard A. Morgan,[1] Philip D. Gregory,[1] Jordan Jarjour,[1] and Alexander Astrakhan[1]

[1]bluebird bio, inc., Cambridge, Massachusetts, USA. [2]Department of Pediatrics, Division of Blood and Marrow Transplantation, University of Minnesota, Minneapolis, Minnesota, USA.

Chimeric antigen receptor (CAR) T cell therapies have achieved promising outcomes in several cancers; however, more challenging oncology indications may necessitate advanced antigen receptor designs and functions. Here we describe a bipartite receptor system composed of separate antigen-targeting and signal transduction polypeptides, each containing an extracellular dimerization domain. We demonstrate that T cell activation remains antigen dependent but can only be achieved in the presence of a dimerizing drug, rapamycin. Studies performed in vitro and in xenograft mouse models illustrate equivalent to superior antitumor potency compared with currently used CAR designs, and at rapamycin concentrations well below immunosuppressive levels. We further show that the extracellular positioning of the dimerization domains enables the administration of recombinant retargeting modules, potentially extending antigen targeting. Overall, this regulatable CAR design has exquisite drug sensitivity, provides robust antitumor responses, and is flexible for multiplex antigen targeting or retargeting, which may further assist the development of safe, potent, and durable T cell therapeutics.

Introduction

Therapies that harness the immune system are transforming cancer care. From antibody-mediated programmed cell death protein 1 (PD-1/PD-L1) checkpoint blockade to chimeric antigen receptor (CAR) T cells, these approaches expand antigen-specific T cells and can efficiently eliminate antigen-positive tumor cells. Unlike checkpoint blockade, CAR T cells target and eliminate target cells directly, enabling treatment of patients lacking HLA-presented neoepitopes or preexisting tumor-infiltrating lymphocytes (1). Multiple clinical trials are underway to test CAR T cell efficacy in diverse hematologic and solid tumor indications, with the most promising results coming from trials targeting $CD19^+$ or B cell maturation antigen–positive ($BCMA^+$) cancers (2). Long-term remission rates as high as 50% have been reported in patients receiving CAR T therapy and the first two CD19-targeting CAR therapies were granted FDA approval in 2017 for particular B cell cancers (3–6).

Despite encouraging early clinical responses, safety and efficacy remains a challenge for CAR T cell therapies (7). Many CAR T cell responses are associated with antigen-induced cytokine release syndrome (CRS) of varying severity (8). CAR T cells targeting CD19 can also cause severe neurotoxicity, increased risk of infection, and chronic B cell aplasia requiring prolonged intravenous immunoglobulin (IVIG) replacement therapy (3, 4, 9, 10). These safety concerns are not constrained to hematopoietic cancers, as clinical trials in other oncology indications have reported excessive and occasionally lethal CAR T cell activity due to antigen expression on normal tissue (7). Following CAR T cell treatment, disease relapses can occur due to antigen escape, T cell exhaustion, or CAR-directed immune rejection (11–14). Even with excellent potency, these properties may limit the success of CAR T cell therapies to a small number of indications.

Most clinically relevant features of CAR T cell biology, including expansion, biodistribution, effector and memory formation are regulated, directly or indirectly, through antigen receptor signaling. Most CAR constructs are typically composed of a single-chain antibody variable domain (scFv) coupled via hinge and transmembrane-spanning motifs to intracellular costimulatory and activation domains (1, 8). This design drives continuous T cell activation as long as antigen-positive cells are present. In the case of CD19-directed therapies, patients with high tumor burden experience greater initial CAR T cell expansion and become

Conflict of interest: All authors, except BRB, are employees and shareholders of bluebird bio. WHL, JG, MTC, JJ, and AA are co-inventors on patent applications describing the DARIC technology. BRB receives remuneration as an advisor to Kamon Pharmaceuticals, Inc, Five Prime Therapeutics Inc, Regeneron Pharmaceuticals, Magenta Therapeutics and BlueRock Therapeuetics; research support from Fate Therapeutics, RXi Pharmaceuticals, Alpine Immune Sciences, Inc, Abbvie Inc., Leukemia and Lymphoma Society, Childrens' Cancer Research Fund, KidsFirst Fund and is a co-founder of Tmunity.

Submitted: August 23, 2018
Accepted: April 23, 2019
Published: June 6, 2019.

Reference information: *JCI Insight*. 2019;4(11):e124430. https://doi.org/10.1172/jci.insight.124430.

at risk for developing severe CRS and associated sequelae due to fulminant T cell activation (15). Because tumor cellularity is extremely variable within and across tumor types and indications, CAR T therapies have disparate pharmacokinetic properties that are difficult to predict and that do not correlate well with the initial dose (15, 16). Further, in contrast with sterilizing immune responses that eliminate antigen, continuous antigen exposure in a setting of chronic infection or cancer is known to drive a progressive loss of T cell effector function, culminating in exhaustion and defective memory formation (17, 18). Similarly, persistent exposure to CD19 antigen drove T cell exhaustion in a syngeneic mouse with constitutively active CD19-CAR T cells (19). The inability to control CAR T cell activation following infusion substantially impacts safety and potentially limits antitumor responses. Improved CAR architectures, in particular designs that circumvent constitutive antigen-dependent signaling, may be necessary for CAR T cells to successfully address complex and heterogeneous solid and liquid tumors.

Novel CAR designs that allow for controlled T cell activation have been described and vary from universal epitope-specific to small-molecule-regulated CARs (20–24). In addition, CARs that target tumors using separately infused antibodies are in early-stage clinical trials (25). Here, we describe a controllable and adaptable antigen recognition system termed dimerizing agent–regulated immunoreceptor complex (DARIC). We show that DARIC T cells drive highly potent in vitro and in vivo antitumor responses even at subimmunosuppressive rapamycin dosing. By providing a "plug-in" — a recombinant subunit containing a separate scFv-based targeting domain — we show extended functionality and targeting of DARIC T cells to a second antigen. We also demonstrate that DARIC T cells can be re-activated following extended periods of drug cessation. DARIC is thus a highly customizable and potent signaling architecture for next-generation T cell therapy applications that is easily toggled between on and off states using rapamycin.

Results

CD19-DARIC component design. We initially developed DARIC constructs targeting the human CD19 antigen for comparison with well-characterized CD19 CAR T cells. The CD19-DARIC has a split-receptor design segregating the antigen-binding and intracellular signaling subunits into 2 membrane-tethered polypeptides that dimerize in the presence of rapamycin. The antigen recognition subunit contains an N-terminal CD19-targeting scFv (clone FMC63) fused to the FK506-binding protein (FKPB12) and a CD4 transmembrane domain. The physically separated signaling subunit contains the FKBP-rapamycin binding (FRB*) (26) domain from the human mTOR complex fused to the CD8α transmembrane domain, followed by the cytoplasmic signaling domains of 4-1BB and CD3ζ (Figure 1A) (27, 28). For lentiviral expression, the 2 components are linked by a porcine teschovirusvirus-1 2A (P2A) peptide and placed under the control of the myeloproliferative sarcoma virus enhancer, negative control region–deleted, dl587rev primer-binding site–substituted U3 (MNDU3) promoter. In the absence of rapamycin ("OFF" state), CD19-DARIC T cells may bind $CD19^+$ target cells but do not initiate signal transduction due to the disconnect between the antigen-binding and intracellular signaling subunits. Addition of rapamycin, or the nonimmunosuppressive rapalog AP21967 (26), dimerizes the 2 subunits to form a signaling-competent immunoreceptor complex ("READY" state). A second-generation CD19-CAR construct containing the identical scFv and a 4-1BB-CD3ζ signaling domain was used as a control in all experiments (Figure 1B).

CD19-DARIC expression and T cell characterization. The CD19-CAR and CD19-DARIC T cells were characterized prior to tumor coculture. Antibody-activated peripheral blood mononuclear cells (PBMCs) were left untransduced (UTD) or transduced with lentiviral vectors and expanded over 10 days followed by characterization of the T cell products. Both CD19-CAR and CD19-DARIC T cells had similar ex vivo expansion following lentiviral transduction (data not shown). We next determined the cell surface phenotype of the transduced T cells. It has previously been shown that antigen-independent T cell activation (tonic signaling) results in downregulation of CD62L expression (29, 30). Using the CD45RA and CD62L expression profile, we observed a similar phenotype for UTD cells and for CD19-CAR or CD19-DARIC T cells, suggesting that CD19-DARIC expression does not lead to tonic signaling (Figure 1C).

Both CD19-CAR and CD19-DARIC T cells had similar numbers of viral integrations as determined by vector copy number (VCN) analysis (CD19-CAR VCN 3.7 and CD19-DARIC VCN 3.1; mean of 3 transductions). Interestingly, CD19-DARIC T cells demonstrated significantly reduced binding of fluorescently labeled recombinant CD19 antigen compared with CAR T cells (Figure 1D, MFI values in red). The decreased staining pattern could be due to lower transgene expression, DARIC instability in the absence of dimerizing agent, inefficient scFv export to the plasma membrane, or steric blockade of scFv binding

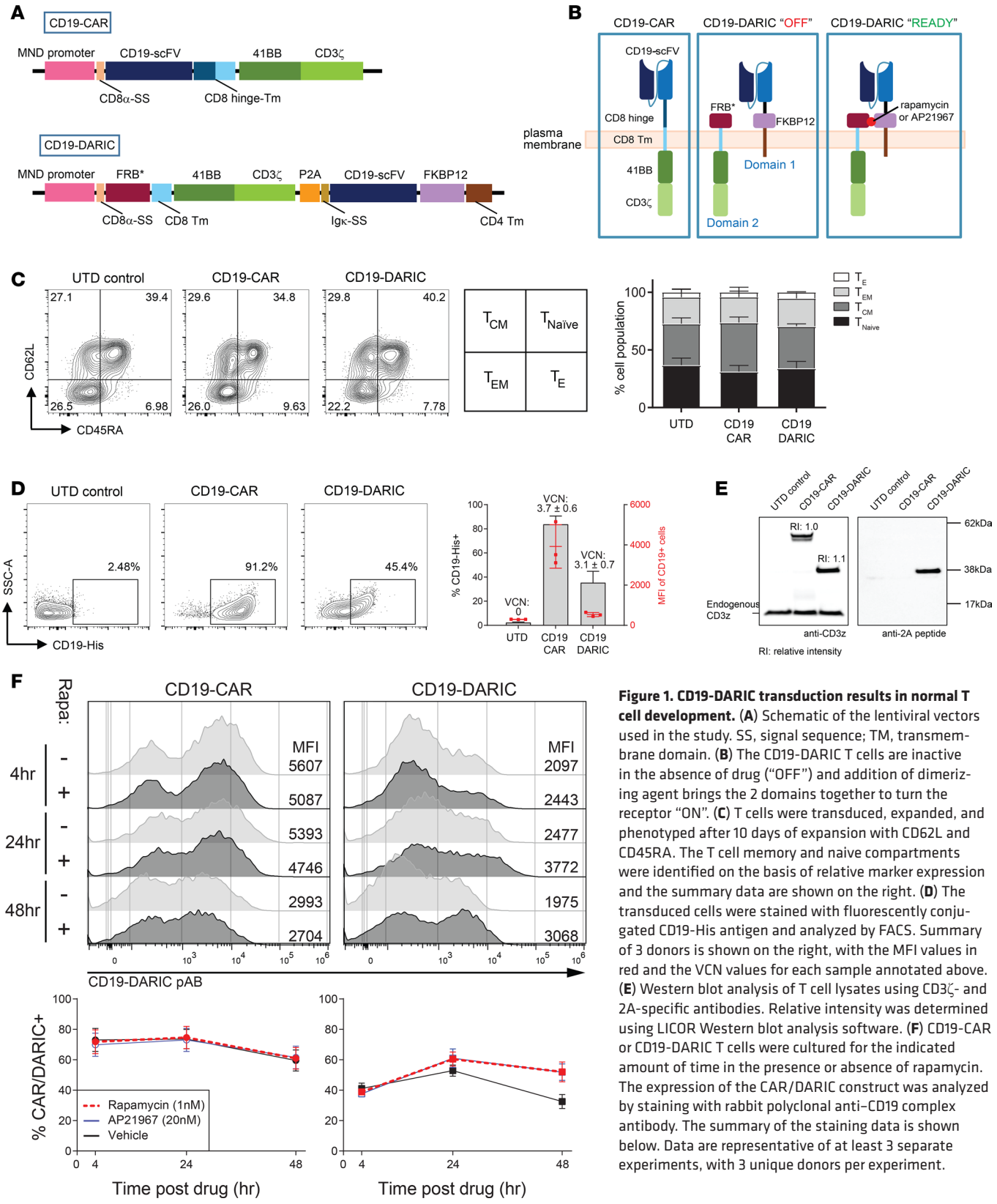

Figure 1. CD19-DARIC transduction results in normal T cell development. (**A**) Schematic of the lentiviral vectors used in the study. SS, signal sequence; TM, transmembrane domain. (**B**) The CD19-DARIC T cells are inactive in the absence of drug ("OFF") and addition of dimerizing agent brings the 2 domains together to turn the receptor "ON". (**C**) T cells were transduced, expanded, and phenotyped after 10 days of expansion with CD62L and CD45RA. The T cell memory and naive compartments were identified on the basis of relative marker expression and the summary data are shown on the right. (**D**) The transduced cells were stained with fluorescently conjugated CD19-His antigen and analyzed by FACS. Summary of 3 donors is shown on the right, with the MFI values in red and the VCN values for each sample annotated above. (**E**) Western blot analysis of T cell lysates using CD3ζ- and 2A-specific antibodies. Relative intensity was determined using LICOR Western blot analysis software. (**F**) CD19-CAR or CD19-DARIC T cells were cultured for the indicated amount of time in the presence or absence of rapamycin. The expression of the CAR/DARIC construct was analyzed by staining with rabbit polyclonal anti–CD19 complex antibody. The summary of the staining data is shown below. Data are representative of at least 3 separate experiments, with 3 unique donors per experiment.

due to the presence of FKBP12. To investigate this, we performed Western blot analysis of CD3ζ expression in total lysates, which showed similar CD3ζ levels in CD19-CAR and CD19-DARIC T cells (Figure 1E). We also used a 2A-specific antibody to probe the efficiency of 2A skipping in the DARIC system. In a complete ribosome skipping process, the 2A peptide remains at the C-terminus of the CD3ζ signaling domain, producing a 38-kDa polypeptide (31). Incomplete ribosome skipping will result in the formation of a high-molecular-weight fusion protein detectable with the 2A-specific antibody (31). A single 38-kDa band was detected in DARIC cell lysates, confirming an efficient ribosomal skipping process and suggesting that uncleaved DARIC fusions are unlikely to account for reduced antigen staining (Figure 1E). Previous studies have shown that both FRB* and FKBP12 can be unstable and degraded in the absence of rapamycin (32, 33); however, preincubation with rapamycin or AP21967 did not change the CD19-His binding pattern (data not shown). Because antigen binding may be sterically hindered by the presence of the FKBP12 domain, we raised rabbit polyclonal antibodies directed against the FRB-rapamycin-FKBP12-CD19 complex to determine whether addition of a dimerizing agent can stabilize complex formation. The polyclonal antibodies recognized CD19-scFv and could be used to stain both CD19-CAR and CD19 DARIC T cells. Addition of either AP21967 or rapamycin had minimal impact on CD19-CAR expression (Figure 1F). However, extended culture of CD19-DARIC T cells in the presence of either AP21967 or rapamycin resulted in increased staining using the polyclonal antibody (Figure 1F). Combined, these data suggest that differential surface staining of CD19-DARIC is not due to reduced transgene expression but rather due to a combination of protein instability and possibly steric hindrance blocking the CD19-His interaction.

Rapamycin drives antigen-dependent CD19-DARIC activation. The CD19$^+$ acute lymphoblastic leukemia–derived (ALL-derived) Nalm-6 cell line was used for in vitro and in vivo testing of CD19 CAR and CD19-DARIC T cells. Initially, T cells were cocultured with GFP$^+$ Nalm-6 cells at a 1:1 effector to target (E/T) ratio for 24 hours in the presence of various concentrations of rapamycin or AP21967 and IFN-γ concentration in the supernatant was analyzed using ELISA. CD19-CAR T cells, but not UTD controls, produced IFN-γ when cocultured with Nalm-6 target cells. We detected minimal cytokine secretion when CD19-DARIC T cells were exposed to Nalm-6 cells without dimerizing drug. However, when CD19-DARIC T cells were cocultured with Nalm-6 in the presence of rapamycin or AP21967, we observed equivalent or even greater levels of IFN-γ secretion compared with CAR controls. Notably, initial rapamycin or AP21967 titration experiments had minimal dose response, with a cytokine production plateau at the lowest dose (Figure 2, A and B). We titrated the rapamycin concentration further to determine if CD19-DARIC T cells still respond at low rapamycin dosing. Rapamycin, but not AP21967, reduced CAR-mediated cytokine production in a concentration-dependent manner (Figure 2C). Interestingly, CD19-DARIC T cells were activated at low rapamycin concentrations and produced higher cytokine levels compared with CD19-CAR T cells when cultured with AP21967 or low rapamycin doses (Figure 2C). Neither the CAR nor DARIC T cells showed substantial cytokine production in the absence of target cells, even in the presence of rapamycin (data not shown).

We used a FACS-based cytotoxicity assay to analyze the lytic activity of CAR and DARIC T cells. While CAR T cells eliminated 85% of GFP$^+$ Nalm-6 cells in a 24-hour coculture assay, CD19-DARIC T cells had minimal cytotoxicity (~20%) in the absence of rapamycin or AP21967 (Figure 2D). Addition of rapamycin (1 nM) or AP21967 (20 nM), however, produced equivalent levels of cytotoxicity of CD19-CAR T cells (~80%, Figure 2D). We also used live-cell imaging to analyze the kinetics of tumor cell killing with CD19-CAR or CD19-DARIC samples. The adherent A549 tumor line was stably transduced with CD19 and a red reporter and cultured with CD19-CAR or CD19-DARIC cells in the presence or absence of dimerizing agents. Tumor growth was analyzed by IncuCyte live-cell imager. The A549 cells grew normally in the presence of rapamycin or UTD T cells, while coculture with CD19-CAR T cells resulted in tumor elimination (Supplemental Figure 1A; supplemental material available online with this article; https://doi.org/10.1172/jci.insight.124430DS1). The CD19-DARIC T cells exhibited some antigen-specific cytotoxicity in the absence of rapamycin; however, addition of either rapamycin or AP21967 resulted in equivalent cytotoxicity compared with CD19-CAR controls. Notably, the CD19-CAR and CD19-DARIC T cells exhibited similar cytotoxicity kinetics in the presence of dimerizing drug, suggesting that the dimerization process does not delay T cell activation. Similar to the data shown in Figure 2, A–C, the activity of CD19-CAR T cells was slightly suppressed by rapamycin, while CD19-DARIC T cells exhibited equivalent cytotoxicity in the presence of either rapamycin or AP21967. As expected, we saw no cytotoxicity with either CD19-CAR or CD19-DARIC T cells when cultured with A549 cells transduced with a control BCMA antigen (Supplemental Figure 1B).

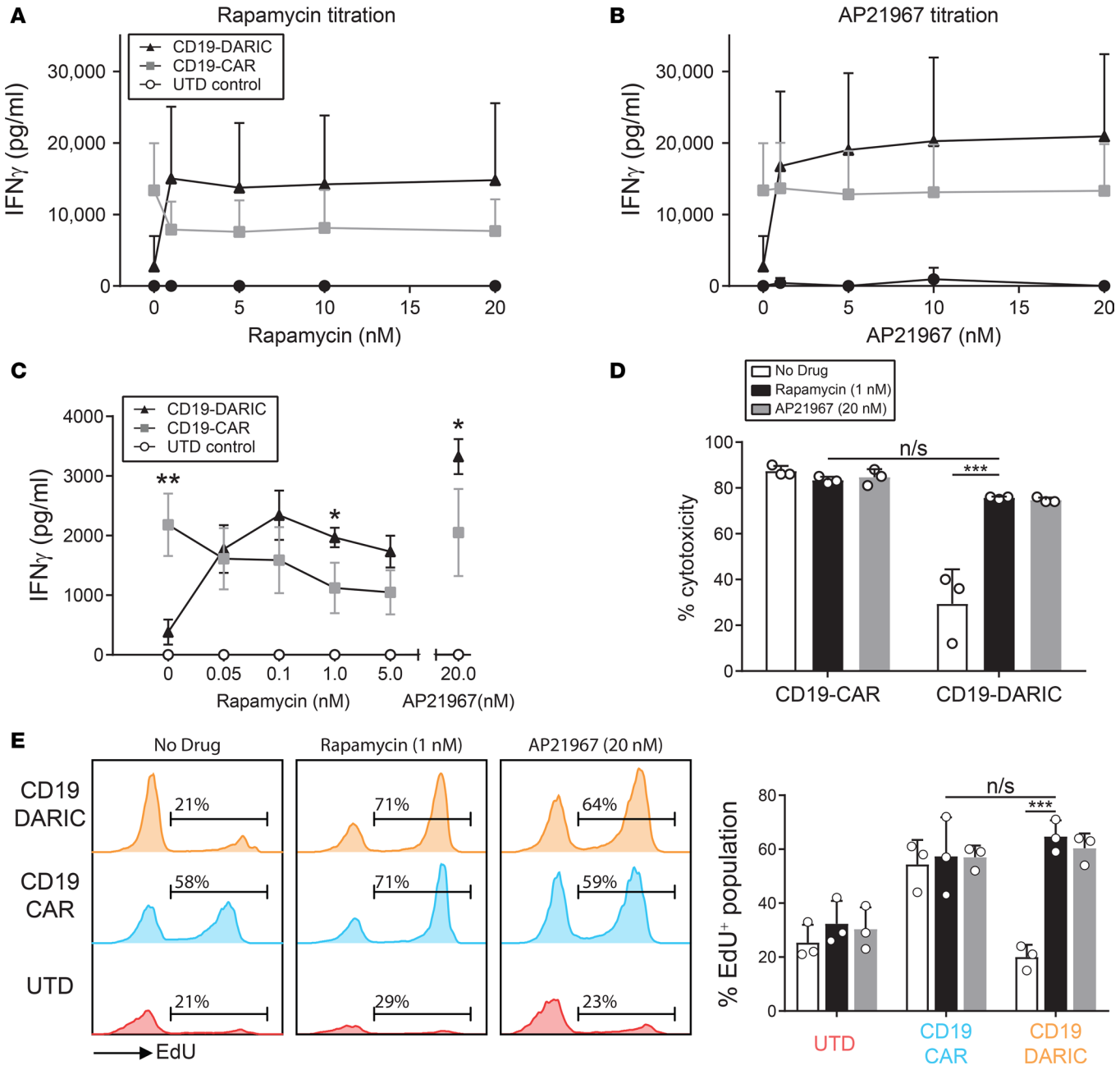

Figure 2. CD19-DARIC T cells are tumor reactive solely in the presence of a dimerization drug. (**A**–**C**) The CD19-CAR and CD19-DARIC T cells were cultured at a 1:1 ratio with fluorescent Nalm-6 target cells with or without different concentrations of either rapamycin or AP21967. Supernatant was collected 24 hours after culture initiation and cytokine levels were analyzed using IFN-γ–specific ELISA (**A** and **B**) or iQue QBead assay (**C**) ($n = 3$). $^{*}P < 0.05$; $^{**}P < 0.01$ as determined by a 2-tailed unpaired Student's t test. (**D**) The percentage cytotoxicity was determined by analyzing the ratio of fluorescent Nalm-6 cells to antigen-naive K562 cells following a 24-hour coculture with CAR or DARIC T cells. (**E**) The T cells were cocultured with Nalm-6 for 72 hours in the indicated conditions. Modified EdU was added and the cells were cultured for another 24 hours prior to analysis of EdU incorporation. The percentage of EdU^{+} cells represents the proportion of cells that underwent DNA synthesis in the prior 24 hours. $^{***}P < 0.001$ using 1-way ANOVA with Dunnett's test for multiparameter comparison to CD19-DARIC T cells cultured with rapamycin. n/s, not significant.

Using incorporation of 5-ethynyl-2′-deoxyuridine (EdU) as a surrogate readout of T cell proliferation, we detected similar proliferation levels for both CD19-CAR and CD19-DARIC T cells when cultured in the presence of Nalm-6 targets and rapamycin. However, CD19-DARIC T cells had minimal EdU uptake when cultured in the absence of a dimerizing agent (Figure 2E). Combined, these findings demonstrate that the DARIC signaling architecture displayed a minimal basal activity and only gains signaling competency in the presence of a dimerization agent.

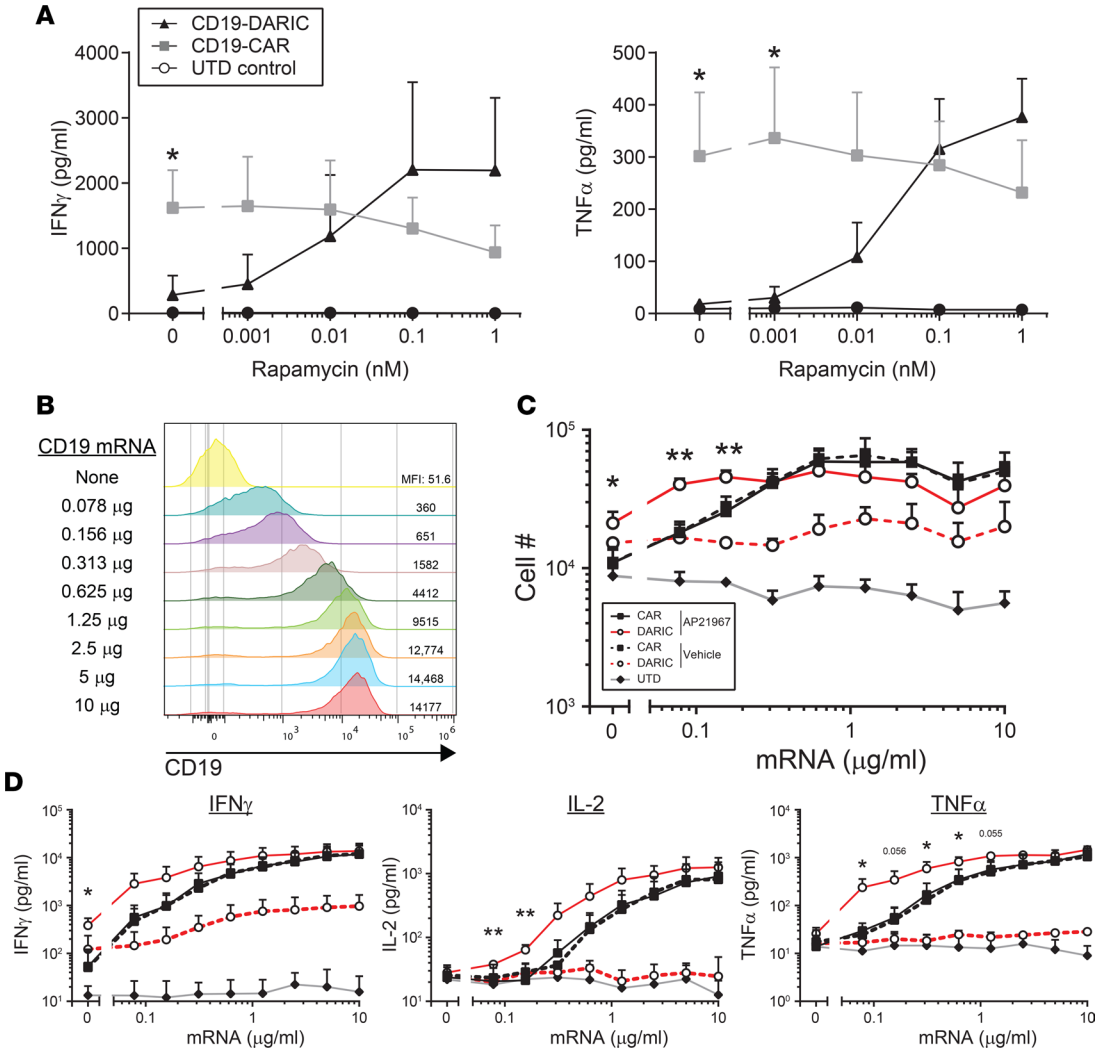

Figure 3. CD19-DARIC T cells are potent even at low rapamycin concentrations and low antigen expression. (**A**) CD19-DARIC or CD19-CAR T cells were cultured with Nalm-6 cells for 24 hours in the presence of different concentrations of rapamycin. Cytokine production was analyzed using iQue QBeads. Data points represent 3 donors. (**B**) K562 cells were transfected with in vitro–transcribed mRNA encoding the CD19 antigen. The transfected cells were cultured for 24 hours and CD19 expression was analyzed by flow cytometry. The amount of CD19 mRNA for each transfection is shown on the left, and the CD19 MFI value is listed on the right. (**C**) CD19-transfected K562 cells were cultured with CD19-DARIC (red) or CD19-CAR (black) T cells in the presence of 20 nM AP21967. After a 24-hour incubation period, supernatant was collected for cytokine analysis and cells were cultured for an additional 72 hours (4 days total coculture). At the conclusion of the coculture period, the number of T cells in each well was counted. The dashed lines represent samples cultured without AP21967, while solid lines represent samples cultured in the presence of 20 nM AP21967. The gray line indicates untransduced control. (**D**) Cytokine production in 24-hour supernatants from **C** was analyzed using iQue QBeads. Data points represent 3 unique donors. $*P < 0.05$; $**P < 0.01$ as determined by a 2-tailed, unpaired Student's *t* test comparing AP21967-treated CD19-DARIC T cells versus AP21967-treated CD19-CAR samples.

Rapamycin drives antigen-dependent elimination of ALL-derived B cell lines. ALL is a highly heterogeneous disease with different levels of CD19 expression, multiple potential genetic alterations, and various ways to block immune recognition of the tumor. We tested the responsiveness of CD19-CAR and CD19-DARIC T cells to various ALL-derived tumor cell lines that expressed different amounts of CD19 antigen (Supplemental Figure 2A). The CD19-CAR T cells secreted cytokines when cocultured with all the ALL tumor cell lines. Notably, the CD19-DARIC T cells did not produce cytokines when cultured with tumor cells alone. However, with the exception of the GM20390 cell line, addition of either rapamycin or AP21967 induced considerable cytokine production, with cytokine secretion levels positively correlated to CD19 expression (Supplemental Figure 2B). As expected, addition of rapamycin was immunosuppressive to CD19-CAR T cells, with reduced cytokine production compared with rapamycin-treated CD19-DARIC T cells for nearly all the cell lines (Supplemental Figure 2B).

The CD19-DARIC T cells are active at low rapamycin dosing and recognize minimal amounts of CD19 antigen. The typical rapamycin clinical dose results in a trough rapamycin concentration of 3–15 nM (34). To determine if CD19-DARIC T cells would be primed by subclinical rapamycin concentrations, CD19-DARIC T cells were cocultured with Nalm-6 cells in the presence of different concentration of rapamycin. Notably, even a very low rapamycin concentration (1 pM) induced some antigen-mediated cytokine production from CD19-DARIC T cells (Figure 3A). Cytokine production increased with higher rapamycin concentration, plateauing at 100 pM, suggesting that CD19-DARIC T cells are active at subclinical rapamycin concentrations.

The expression of CD19 is a key variable for effective CAR response, and CD19 antigen downregulation can mediate tumor escape and the loss of CD19-CAR activity (11). Surprisingly, in vitro experiments showed higher cytokine production from CD19-DARIC T cells compared with CD19-CAR T cells (Figure 2 and Supplemental Figure 2). To determine if CD19-DARIC T cells were more sensitive to CD19 antigen expression, $CD19^-$ K562 cells were transfected with different amounts of CD19 mRNA. After 24 hours, the transfected K562 exhibited a concentration-dependent range of CD19 expression (Figure 3B). The K562 cells were cocultured with CD19-CAR or -DARIC T cells for an additional 24 hours in the presence of the dimerizing agent AP21967 and supernatants were collected for cytokine analysis. The coculture was continued for 3 additional days to analyze antigen-induced T cell proliferation. At the conclusion of the coculture (4 days after activation), the number of T cells in each sample was counted (Figure 3C). There was no CD19-DARIC T cell expansion in the absence of AP21967, even at very high levels of CD19 expression. Conversely, CD19-CAR T cells exhibited antigen-dose-dependent T cell growth, with similar proliferation rates in the presence or absence of AP21967. Interestingly, CD19-DARIC T cells had some, albeit minimal, cell growth when cultured with AP21967 alone. However, coculture of CD19-DARIC T cells with both AP21967 and K562-CD19 target cells resulted in antigen-dependent increase in T cell proliferation. There was a significantly higher expansion of CD19-DARIC T cells compared with CD19-CAR T cells, but only at the low CD19 dose levels (Figure 3C), with CD19-CAR and CD19-DARIC expansion plateauing at higher antigen densities. We observed a similar pattern with cytokine production, with generally higher level of cytokine production from CD19-DARIC T cells at all levels of CD19 expression (Figure 3D). Higher cytokine production was particularly notable at low CD19 expression for all cytokines tested. Combined, these data demonstrated exquisite sensitivity of CD19-DARIC T cells to both rapamycin concentration and antigen expression and suggest that CD19-DARIC T cells are more likely to respond to low antigen expression compared with CD19-CAR T cells.

DARIC plug-in expands antigen-recognition diversity of CAR T cells. The extracellular positioning of the FRB domain in the DARIC system means that this domain is potentially available to partner with other extracellular FKBP12-containing antigen-binding components. We explored whether a secondary FBKP12-conjugated scFv, termed DARIC plug-in, can broaden the antigen reactivity of CAR T cells (Figure 4A). We made recombinant plug-in proteins targeting CD19 (Figure 4B) and BCMA (not shown). The plug-in protein was produced in 293T cells and used without further purification or purified using an FKBP12 affinity column. We tested the potential utility of the plug-in in 2 different DARIC applications.

First, we tested whether the BCMA plug-in is able to provide secondary antigen specificity for CD19-DARIC T cells. The BCMA plug-in is a previously described BCMA-specific scFv (35) conjugated to FKBP12. We cultured CD19-DARIC T cells with $BCMA^+$ K562 cells, either alone or in the presence of rapamycin. As expected, we saw minimal cytokine production with or without rapamycin. Addition of a rapamycin-prebound BCMA plug-in, however, resulted in antigen-specific cytokine production. This was a dose-dependent finding, as more recombinant BCMA plug-in led to high levels of cytokine secretion (Figure 4C). Next, we reversed this approach and used a BCMA-specific DARIC with a CD19 plug-in. The BCMA-DARIC construct is similar in design to the CD19-DARIC but utilizes a BCMA-specific scFv (35). We took cultures of BCMA-DARIC in the "off position" without the addition of rapamycin and added the CD19 plug-in that had been prebound with rapamycin and cultured these cells with $BCMA^-CD19^+$ Nalm-6 cells. Analysis of coculture cell media 24 hours later demonstrated successful redirection of BCMA-DARIC T cells to target Nalm-6 cells using the CD19 plug-in (Figure 4, D and E).

Next we modified a standard BCMA CAR by inserting an FRB* domain between the scFv and CD8α-hinge region (Figure 4F). These T cells, termed adaptable-CAR T cells, retain the antigen specificity of parental BCMA-CAR T cells as determined with cytotoxicity and cytokine production assays (Figure 4, G and H). To determine if the CD19 plug-in can function in this context, we added rapamycin-bound CD19 plug-in to cultures and set up a Nalm-6 coculture. As expected, neither BCMA-CAR nor BCMA-adaptable-CAR T cells exhibited functional responses to BCMA-negative Nalm-6 cells.

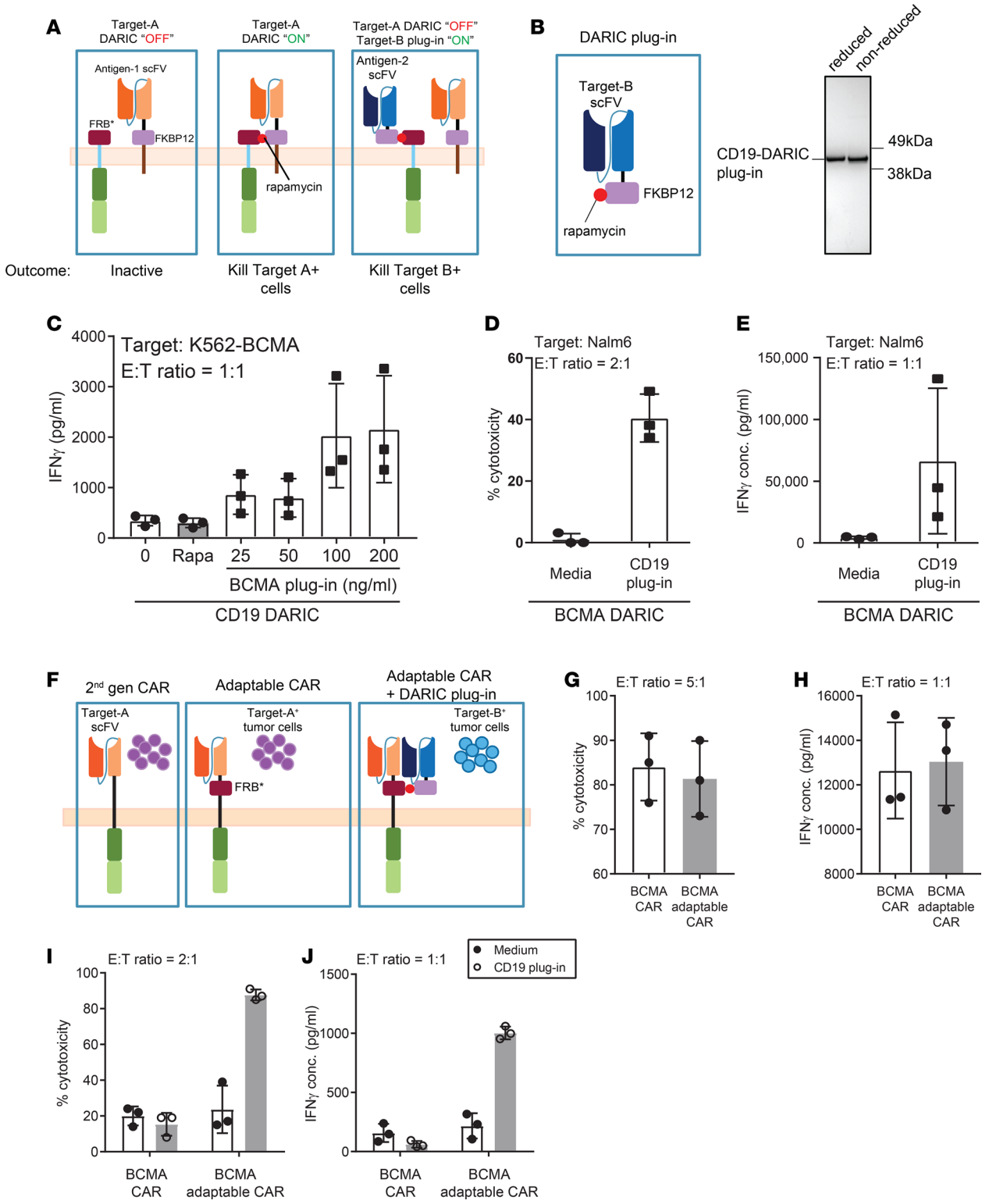

Figure 4. DARIC T cells recognize secondary antigens through the DARIC plug-in system. (**A**) Schematic of a DARIC signaling architecture in the presence or absence of a DARIC plug-in targeting a secondary antigen. (**B**) The recombinant CD19-DARIC plug-in was produced and purified from 293T cells using a rapamycin-based affinity column. The purified protein was analyzed using Coomassie blue staining. (**C**) Unmodified CD19-DARIC T cells were cocultured with K562-BCMA cells alone, in the presence of rapamycin, or in the presence of increasing concentration of rapamycin-preloaded BCMA plug-in. Cytokine production was analyzed by iQue QBeads. (**D**) The cytotoxicity and (**E**) cytokine production of BCMA-DARIC T cells cocultured with CD19$^+$ Nalm-6 cells in the presence or absence of rapamycin-preloaded CD19 DARIC plug-in. (**F**) Schematic of adaptable CAR architecture, with an extracellular FRB* domain located next to the scFv able to bind recombinant DARIC plug-in scFv to target a secondary antigen. (**G**) The cytotoxicity and (**H**) IFN-γ cytokine production of BCMA-adaptable CAR following 24-hour coculture with K562-BCMA target cells was analyzed by FACS and QBeads, respectively. (**I**) The cytotoxicity and (**J**) cytokine production of control and BCMA-adaptable CAR in the presence of recombinant CD19-DARIC plug-in was analyzed after 24-hour coculture with Nalm-6 target cells. Data points represent 3 different donors.

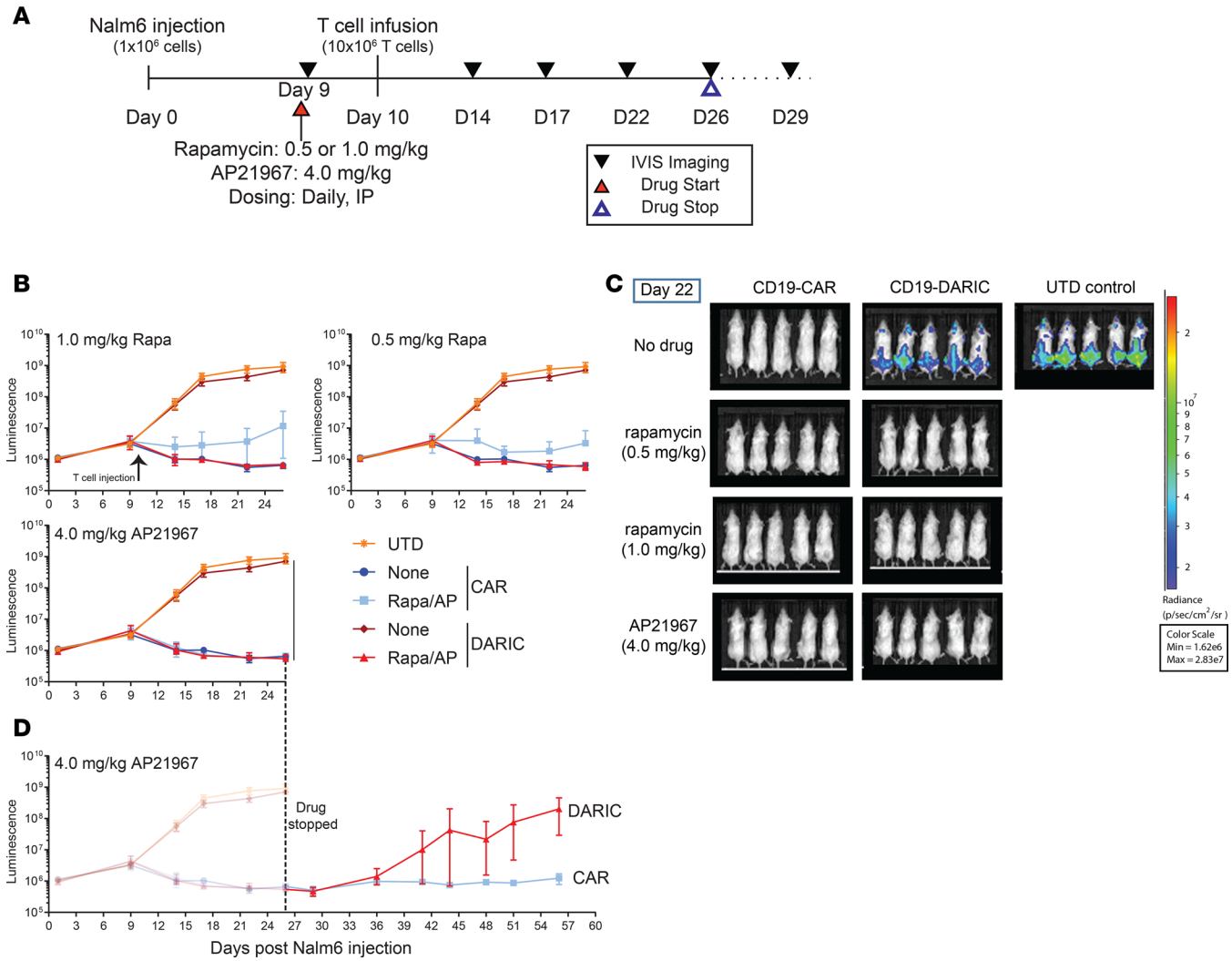

Figure 5. DARIC T cells exhibit drug-mediated tumor control in vivo. (**A**) Outline of the in vivo experiment for testing CD19-DARIC T cells. The T cells were infused 11 days following tumor injection while drug dosing started 1 day prior to T cell injection. (**B**) Summary bioluminescence data for each drug control group. The UDT and the no-drug CAR/DARIC groups are the same for all figures, while the "+ drug" groups (light blue and red) represent the specific drug dose used for the group. Data points represent 5 mice. (**C**) Representative bioluminescence imaging at day 22 following tumor injection. (**D**) Bioluminescence tumor imaging of the AP2167 group followed for additional 20 days after drug dosing was stopped.

However, addition of recombinant CD19 plug-in (1.25 μg/ml) to BCMA-adaptable-CAR T cells, but not to BCMA-CAR T cells, induced cytotoxic and cytokine responses to CD19⁺ Nalm-6 cells in tumor cocultures (Figure 4, I and J). Combined, these findings demonstrate that DARIC T cells can be redirected to target a different antigen by rapamycin-ready DARIC plug-in molecules.

DARIC T cells exert effective in vivo tumor control induced by rapamycin or AP21967. To evaluate the in vivo antitumor efficacy of CD19-DARIC T cells, we established a xenograft mouse model using NOD-SCID-IL2Rgc gamma (NSG) mice injected with Nalm-6 stably expressing firefly luciferase (Nalm6-FFluc). A 1×10^6 dose of Nalm6-FFluc cells was injected intravenously (i.v.) into NSG mice on day 1, and 1×10^7 total T cells were injected i.v. on day 10, after tumor engraftment was confirmed via bioluminescence. Starting on day 9, mice were given daily i.p. injections of vehicle (DMSO), rapamycin (0.5 or 1 mg/kg), or AP2167 (4 mg/kg). Bioluminescence analysis of tumors grown was performed every 3 or 4 days (Figure 5A). The CD19-CAR or CD19-DARIC T cells had a similar cellular phenotype prior to injection (Figure 1E).

Similar tumor burden was seen in mice that received Nalm-6–FFluc alone, Nalm-6–FFluc with rapamycin/AP21967, or Nalm-6–FFluc with UTD T cells. Conversely, treatment with CD19-CAR T cells led to rapid and sustained decrease in Nalm-6 tumor burden (Figure 5B, dark blue). Consistent with the immunosuppressive effect of rapamycin, rapamycin treatment of CD19-CAR T cells slightly reduced Nalm-6 tumor control in vivo (Figure 5B, light blue).

The in vivo activity of CD19-DARIC T cells was completely dependent on rapamycin. In the absence of drug, mice treated with CD19-DARIC T cells had no appreciable decrease in tumor burden (Figure 5B, purple). However, administration of rapamycin or AP21967 resulted in equivalent levels of tumor clearance compared to mice receiving CD19-CAR T cells (Figure 5B, red curve). Notably, the level of tumor control was similar with all the tested doses of rapamycin or AP2167. No immunosuppressive effect of rapamycin was observed with CD19-DARIC T cells (Figure 5, B–D), even when comparing mice that received rapamycin or the nonimmunosuppressive AP2167 rapalog (Figure 5B vs. 5D).

We investigated whether the activity of CD19-DARIC T cells could be modulated by stopping drug treatment. The AP2167 dosing was stopped after 26 days and the animals were monitored for tumor recurrence for an additional 30 days. While Nalm-6 levels were unchanged in mice treated with CD19-CAR T cells, CD19-DARIC mice had detectable tumor growth less than 7 days after AP21967 was stopped (Figure 5D). These results suggest that the antitumor response of DARIC T cells can be regulated using controlled drug dosing.

DARIC T cells control tumors in vivo at low cell numbers. To determine whether CD19-DARIC T cells are able to control tumor growth at limiting T cell numbers, we infused tumor-bearing mice with different amounts of CD19-CAR or CD19-DARIC T cells. We used the Nalm-6/NSG tumor mice described in Figure 5 for all studies, and a single rapamycin dose (0.2 mg/kg, i.p., daily) was used for all treated mice. All T cell preps had a similar phenotype and CD4/CD8 ratio (Supplemental Figure 3A) and were dosed on the basis of CAR/DARIC positivity (Supplemental Figure 3B). As expected, CD19-CAR, but not CD19-DARIC, controlled tumor growth in the absence of rapamycin. While we did not detect any tumor control with a 1×10^6 CAR/DARIC cell dose, we saw equivalent tumor control for both CAR and DARIC T cells at 5×10^6 and 15×10^6 T cell doses (Supplemental Figure 3C). The 5×10^6 T cell dose exhibited suboptimal tumor control compared with the 15×10^6 cell dose; however, we observed similar clearance kinetics for both dose groups. A single mouse in the 5×10^6 CD19-DARIC dose group had minimal tumor control, suggesting a potential issue with T cell infusion. However, the rest of the individual animals for the 5×10^6 dose had very similar levels of tumor control, suggesting that CD19-CAR and CD19-DARIC exhibit similar levels of activity in vivo even at low T cell dosing (Supplemental Figure 3C).

Nonimmunosuppressive rapamycin dosing drive highly potent CD19-DARIC activity in vivo. In the transplantation setting, rapamycin is typically administered as part of an immunosuppressive cocktail to reduce graft rejection and dampen the immune response. The rapamycin immunosuppressive window corresponds to a 3–15 ng/ml trough level in whole blood (36, 37). While we observed equivalent CD19-DARIC activity in the initial dose titration study, we wanted to perform additional rapamycin titration to determine whether the CD19-DARIC T cells were able to control tumor growth at nonimmunosuppressive rapamycin concentrations. Nalm-6–FFluc cells were inoculated into NSG mice and CD19-DARIC or CD19-CAR T cells were injected on day 10 after tumor inoculation. Mice started receiving daily injections of either 0.1 mg/kg or 0.01 mg/kg rapamycin (q.d.) at 9 days after tumor injection. Alternatively, mice were treated with 0.1 mg/kg rapamycin every other day (q.a.d., Figure 6A). Due to different tumor engraftment kinetics compared with Figure 5, all the mice that received CD19-CAR T cells had detectable Nalm-6 luciferase at all time points, with or without rapamycin treatment (Figure 6B). As seen previously, mice that received CD19-DARIC T cells in the absence of rapamycin had tumor growth equivalent to that of the control group. Strikingly, the CD19-DARIC T cells exhibited complete tumor control and had superior tumor elimination compared with CD19-CAR groups (Figure 6B, red vs. blue lines). Further, the CD19-DARIC groups exhibited similar tumor control at the tested rapamycin doses. We used whole-blood sampling to determine the in vivo rapamycin trough concentration. Whole blood was sampled from all mice 24 hours (q.d.) or 48 hours (q.a.d.) following the last rapamycin dose and rapamycin concentration was determined by liquid chromatography–tandem mass spectrometry (LC-MS/MS). The highest rapamycin dose (0.1 mg/kg, q.d.) produced a 10.4 ng/ml rapamycin trough level, while both the 0.1 mg/kg q.a.d. and 0.01 mg/kg q.d. groups had lower trough concentrations (3.96 ng/ml and 0.7 ng/ml, respectively), with 2 of 5 mice in the 0.01 mg/kg group having rapamycin concentrations below the limit of detection (<1 ng/ml) (Figure 6C). Combined, these findings demonstrate that CD19-DARIC T cells are highly active at nonimmunosuppressive rapamycin dosing and may have superior in vivo activity compared with standard CD19-CAR T cells.

Tunable in vivo tumor control using CD19-DARIC with rapamycin pulsing. Previous data (Figure 5) suggested that CD19-DARIC T cells exert continuous tumor control in the presence of a dimerizing agent and the tumor rebounds once drug dosing is stopped. To test whether the rapamycin dose affects tumor recurrence, drug dosing was stopped 28 days after tumor inoculation and the CD19-DARIC mice were monitored for tumor relapse (Figure 6D). While all drug-treated groups had similar levels of tumor control in the presence

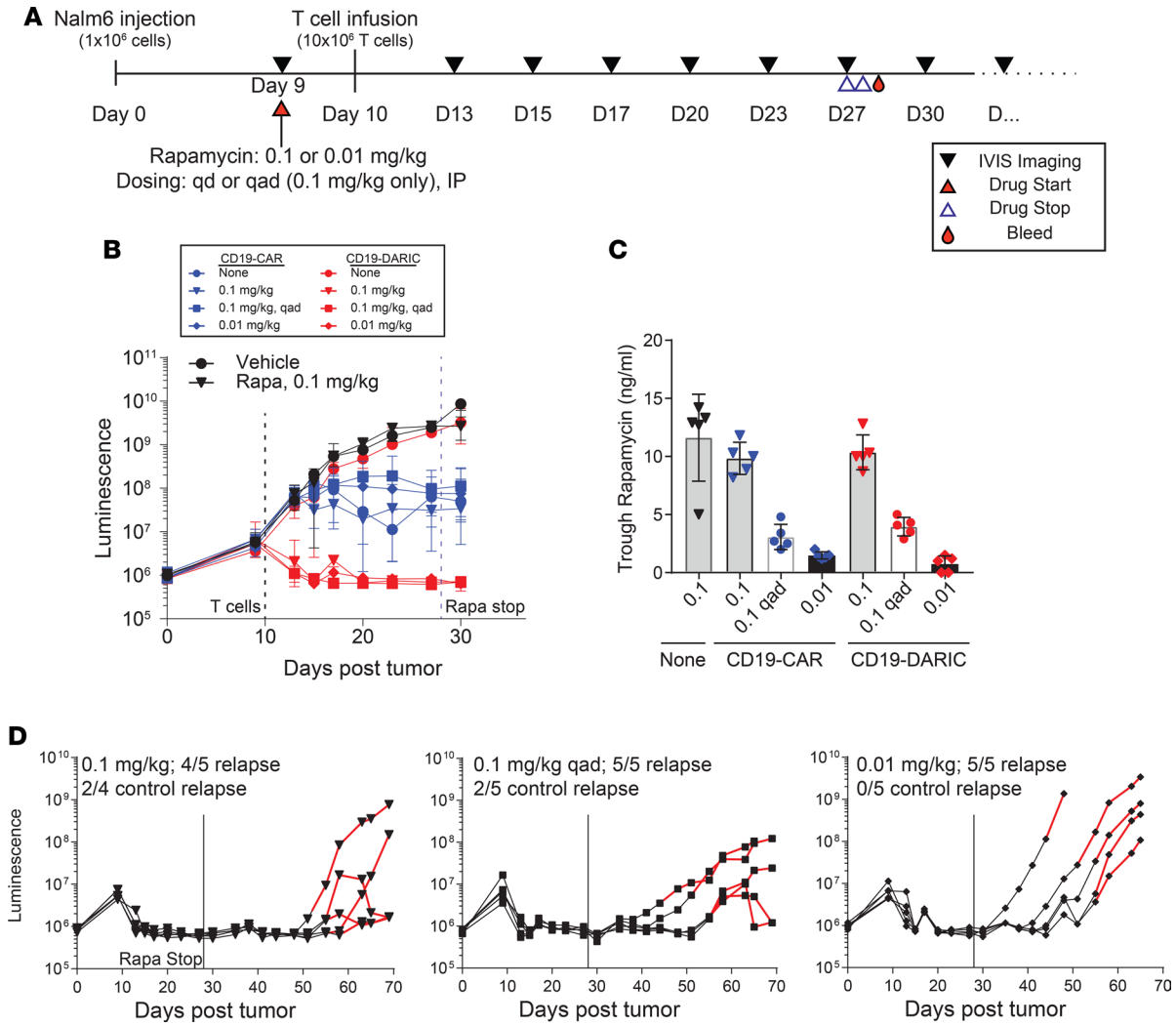

Figure 6. CD19-DARIC T cells control tumor growth in vivo with nonimmunosuppressive rapamycin dosing. (**A**) Outline of the in vivo experiment for analyzing CD19-DARIC activity at low rapamycin dosing. (**B**) Summary bioluminescence reading for all the experimental groups. Black and blue dashed lines represent initial T cell injection and cessation of rapamycin dosing, respectively. Data presented as mean and standard deviation of 5 animals per group. (**C**) Trough rapamycin levels in whole blood were analyzed by liquid chromatography–tandem mass spectrometry (LC-MS/MS). Analysis was done at 24 hours (0.1 and 0.01) or 48 hours (0.1 q.a.d.) following the last rapamycin injection. (**D**) The bioluminescence traces for individual animals from each dose group shown in **B** are represented as black lines. The animals were tracked by regular imaging and rapamycin dosing was restarted when tumor regrowth was detected (red lines).

of rapamycin, all animals treated with the lowest rapamycin dose (0.01 mg/kg) had tumor recurrence within 20 days after drug cessation. Higher rapamycin dosing tended to result in longer remissions (Figure 6D, 0.1 vs. 0.01); however, there was no significant difference in time to relapse between different rapamycin dosing. All the mice in the 0.01 mg/kg q.d. and 0.1 mg/kg q.a.d. group relapsed, while 4 of 5 mice in the 0.1 mg/kg q.d. group relapsed. We monitored each group of mice for tumor recurrence and rapamycin treatment was restarted following a positive luciferase signal (Figure 6D, red lines). While none of the mice in the 0.01 mg/kg q.d. group achieved tumor control after rapamycin re-dosing, 2 of 5 animals in the 0.1 mg/kg q.a.d. group and 2 of 4 mice in the 0.1 mg/kg q.d. group had decreased tumor bioluminescence following rapamycin re-dosing. These observations demonstrate that CD19-DARIC T cells actively suppress tumor growth in the presence of rapamycin and periodic drug re-treatment can re-activate DARIC functionality in vivo.

Discussion

Targeting CD19$^+$ B cell cancers with CAR T cells has produced exceptional clinical outcomes, culminating with the approval of 2 CD19-targeting CAR products within the past 2 years. Consequently, the next generation of CD19 targeting CAR products must produce equivalent or greater efficacy while improving safety

and incorporating multiplex antigen-targeting capacity. The findings presented in this study show that the drug-regulatable DARIC system exhibits similar or greater efficacy in eliminating tumor cells in vitro and in vivo compared with currently used CAR T cell designs. Tumor elimination is fully drug dependent and tumor control is lost once drug dosing is stopped. In addition, we show that the extracellular positioning of the FKBP12 domain enables DARIC T cell retargeting toward additional antigens. Combined, our results establish the DARIC system as a flexible and powerful antigen-targeting platform to create better T cell therapies.

Several other regulatable CAR approaches have been described, including variants that have dimerizable subunits and systems using universal adapter CARs (22, 24, 32, 38). Lim and colleagues designed a system that also uses the FKBP12 and FRB components to regulate CAR activity (22). Unlike DARIC, their approach placed the dimerization domains intracellularly to regulate CAR activity. Intracellular localization of FKBP12 and FRB could hinder or alter signal transduction events and could be susceptible to competition with endogenous FKBP12 and mTOR binding proteins. Consequently, this system required considerably higher dimerizing agent concentrations for activity and did not achieve parity with a CD19 CAR control in vitro or in vivo (22). In addition, Juillerat and coworkers published a rapamycin-regulated system with extracellular positioning of the FRB/FKBP12 dimerizing domains, similar to the DARIC system. Similar to data shown in Figure 1F, the authors showed that rapamycin stabilized expression of an FRB/FKBP12 signaling architecture, while addition of FK506 blocked the dimerization and led to reduced expression. However, they used an FcεRI-based signaling and dimerization architecture and had minimal in vitro and no in vivo functional validation, making it difficult to compare their approach to the DARIC system. Further, the compatibility and efficiency of the DARIC system with the use of rapamycin, a very well-characterized clinical agent, could potentially streamline the translation of the DARIC system to the clinic.

The DARIC plug-in approach expands the potential utility of the DARIC system. We describe 2 different ways to utilize the plug-in approach to retarget T cells toward a second antigen. Notably, both the adaptable CAR and the DARIC approach are compatible with rapamycin-preloaded plug-in proteins. Using rapamycin preloading simplifies clinical use, as rapamycin-prebound plug-in scFvs do not need additional rapamycin to bind the target T cells. Because of the high affinity between FKBP12 and rapamycin (0.2 nM) (39), rapamycin-prebound scFv should not disassociate from rapamycin in vivo, lessening the risk of inadvertent immunosuppression. The kinetics of FKPB12-rapamycin disassociation depend on the availability of DARIC T cells, which will serve as binding and stabilizing partner for the FKBP12-scFv domain. Notably, several adapter-based CAR architectures have been described (21, 24, 40, 41), using a combination of epitope- or linker-based universal CARs. The DARIC architecture combines the antigen flexibility of the universal CAR approach with the functionality and efficacy of traditional single-antigen CAR T cells. This allows potential stepwise development of the DARIC system, starting with a validated CAR target and progressing to secondary antigen targeting once the initial DARIC approach has been clinically tested.

As shown in Figures 5 and 6, CD19-DARIC T cells had similar steady-state antitumor activity at all rapamycin doses tested, and we did not determine the minimal necessary rapamycin dose for complete in vivo response. Partly, this reflects the exquisite sensitivity of the DARIC system even at low rapamycin levels, likely due to the extracellular placement of the dimerization machinery. However, because of this sensitivity, it is difficult to determine the on/off kinetics of the DARIC system in vivo. The CD19-DARIC–treated mice exhibited similar speed and depth of tumor control at all rapamycin doses (Figures 5 and 6). Further, all the treated mice exhibited tumor relapse after cessation of treatment. While the kinetics of relapse may have been faster in animals treated with the lowest dose of rapamycin, these differences were not statistically significant (Figure 6D). Notably, the animals that were able to control the tumor relapse did so rapidly after rapamycin reinitiation, suggesting that the CD19-DARIC system can rapidly turn on after provision of the dimerizing agent. Future experiments using T cell, rapamycin, and FK506 dose titrations will determine the full on/off kinetics of the CD19-DARIC system in steady-state tumor growth versus relapse.

Rapamycin has wide applications in both transplantation and oncology (37, 42). It is available in oral and intravenous formulations and has clearly defined pharmacokinetic and pharmacodynamics properties in both adult and pediatric populations. Because rapamycin has a considerably shorter half-life in mice (~15 hours) (43) compared with adult humans (~60 hours) (42), interpolating clinical dosing from mouse studies is complicated. However, the high activity of CD19-DARIC T cells at all tested doses potentially enables considerable clinical dosing flexibility. Weekly subimmunosuppressive oral rapamycin, higher dose immunosuppressive regimens to promote competitive DARIC T cell engraftment, episodic dosing to

mitigate T cell exhaustion, or the use of alternative rapamycin formulations such as everolimus or temsirolimus, are all potentially available as interventions to fine-tune T cell activation dynamics.

By inhibiting mTOR signaling, rapamycin is broadly immunosuppressive at medium and high doses, impacting all stages of the immune response, including T and B cell activation, antigen presentation, and natural killer responses (44). At the same time, rapamycin treatment has also been shown to enhance $CD8^+$ T cell memory formation by promoting the lipid metabolism pathway at the expense of the glycolytic metabolism used by $CD8^+$ effector cells (45, 46). Notably, rapamycin-mediated T cell memory formation is highly dependent on the dose and timing of rapamycin in the context of a broader immune response (46). Improved responses to immunization and reduced infection rates in elderly patients treated with low-dose everolimus alone or in combination with a catalytic mTOR/PI3K inhibitor have been reported in a clinical trial setting (47). Given these observations and the low rapamycin dose requirements established in our DARIC studies, the rapamycin treatment component of putative DARIC T cell therapies should either have a minimal systemic effect, or may even slightly dampen the broader immune response, modulating the intensity and onset of treatment-related CRS and/or the development of the bystander T cell response.

The formation of a functional T cell memory pool depends on multiple factors, including expression of appropriate costimulatory ligands, favorable nutrient availability, concentrations of cytokines, and, most importantly, the magnitude and duration of antigen-specific T cell response. Persistent and chronic T cell activation may induce T cell exhaustion instead of memory formation (17, 48). Although multiple factors contribute to the failure of CAR T therapies, these cells often exhibit exhaustion characteristics, such as altered metabolism and upregulation of checkpoint markers, in both clinical and preclinical models. Conceptually, persistent antigen exposure within the solid tumor or through continuous generation of $CD19^+$ target cells may result in the development of T cell tolerance or T cell exhaustion due to chronic CAR stimulation (16, 49, 50). Consistent with this idea, chronic antigen exposure resulted in reduced CD19-CAR T cell persistence in a syngeneic mouse model. Incorporating a rest period between antigen exposure, however, led to drastically enhanced CAR expansion in vivo and a reduced CAR exhaustion profile (19). These and other observations suggest that DARIC activation using pulsatile rapamycin dosing may more accurately mimic the endogenous immune response and lead to improved T cell memory formation and reduced risk of exhaustion.

The development of regulatable CAR architectures and safety switches has been partially driven by the severe adverse events (SAEs) occasionally seen in CD19 CAR T cell clinical trials. These SAEs present as either rapid-onset acute manifestation of CRS or more persistent and longer-term neurologic toxicity (9). Other less severe complications from CD19 CAR T cell therapy such as chronic B cell aplasia (3) and increased risk for infections (10) can be divided into short- and long-term effects. Acute CRS-related toxicity typically resolves via infusion of anti–IL-6 antibody (tocilizumab), while neurologic complications take longer to resolve and may have a different underlying mechanism compared with acute CRS (9). Given the sensitivity of the CD19-DARIC system, treatment interruption is not likely to prevent or stop fulminant CRS manifestations. However, a low-dose rapamycin treatment combined with neurotoxicity monitoring should enable rapid dose de-escalation if neurological toxicity is observed, potentially reducing or stopping CAR-mediated neurologic SAEs. As a separate safety mechanism, the FKBP12 component of the DARIC system binds FK506 (tacrolimus) in addition to rapamycin (51). In case of severe CRS or persistent neurotoxicity, FK506 administration should reduce rapamycin binding to FKBP12 through competitive inhibition, thereby lessening DARIC activity while inducing general immunosuppression to further dampen a CRS response (36). We are currently investigating whether FK506 administration is able to modulate CD19-DARIC activity in vitro or in vivo.

In conclusion, the data presented in this study demonstrate the potential of CD19-DARIC T cells for regulated and effective tumor targeting. Unlike other regulatable or apoptosis-based safety systems, the CD19-DARIC approach is just as potent as standard CD19-CAR T cells and can be regulated with clinically relevant rapamycin dosing. These findings support continued development of DARIC T cells for hematopoietic and solid tumor indications.

Methods

Reagents, antibodies, and cell lines. Rapamycin was purchased from Sigma-Aldrich. The nonimmunosuppressive rapamycin analog (rapalog) AP21967 was from TaKaRa. Both AP21967 and rapamycin were resuspended in DMSO and diluted in PBS immediately prior to in vitro or in vivo use. CD19-CAR or CD19-DARIC expression in T cells was detected either by flow cytometry using CD19-HIS PE (Creative Biomart) or by Western blot analysis using rabbit anti-2A polyclonal antibodies (Millipore) and mouse anti–human CD3ζ monoclonal

antibody (Santa Cruz Biotechnology). In vitro T cell subset development was analyzed by flow cytometry with anti-CD62L-APC (clone DREG-56) and anti-CD45RA-PECy7 (clone HI100), both from Biolegend. 293T cells, Nalm-6 cells, and K562 cells were purchased from ATCC. DMEM, RPMI-1640, HEPES, GlutaMax, and fetal bovine serum (FBS) were purchased from Thermo Fisher Scientific. X-VIVO 15 media were purchased from LonzaJ. Human AB sera were from Valley Biomedical. 293T cells were cultured in DMEM supplemented with 10 mM HEPES, 2 mM GlutaMax, and 10% FBS. Nalm-6 and K562 cells were cultured in RPMI-1640 supplemented with 10 mM HEPES, 2 mM GlutaMax, and 10% FBS. T cell growth medium (TCGM) was prepared with X-VIVO 15 supplemented with 10 mM HEPES, 2 mM GlutaMax, and 5% human AB serum.

Lentiviral production. Lentiviral production was performed as previously described (35). Briefly, CD19-CAR (52), CD19-DARIC, BCMA-CAR (35), BCMA-DARIC, and BCMA-adaptable CAR lentiviral constructs were cotransfected with a 3-packaging-vector system into 293T cells using PEIpro reagent (Polyplus). Lentivirus-containing culture supernatants were collected, filtered, aliquoted, and stored at –80°C 48 hours after transfection. VCN analysis was performed as previously described (35).

Human PBMC culture and lentiviral transduction. Cryopreserved PBMCs from healthy donors (Key Biologics) were thawed and cultured in TCGM supplemented with 250 U/ml recombinant human IL-2 (CellGenix) and 50 ng/ml anti-CD3 (clone OKT3) and anti-CD28 (15E8) antibodies (Miltenyi Biotec) on day 0, as previously described (35). Lentiviral supernatant was added to PBMC cultures 24 hours after activation. At 72 hours after activation, transduced PBMCs were collected, washed, and resuspended in complete TCGM with human IL-2 at 0.5×10^6 cells/ml. PBMC cultures were maintained at 0.5×10^6 cells/ml with the addition of fresh media every 2 days. Flow cytometry acquisition was performed using an Attune NxT (Thermo Fisher Scientific) and the data analyzed using FlowJo software (FlowJo, LLC). In vitro functional assays were performed on day 9 and day 10 as described in figure legends.

Western blot analysis. For protein analysis, 2×10^6 T cells were lysed and prepared in NuPAGE LDS sample buffer (Thermo Fisher Scientific), separated with NuPAGE 4%–12% Bis-Tris gels, and then transferred onto nitrocellulose membranes using the iBlot transfer system (Thermo Fisher Scientific). After incubation with 5% nonfat milk in TBST (10 mM Tris, pH 8.0, 150 mM NaCl, 0.5% Tween 20) for 15 minutes, the membranes were incubated with antibodies against 2A peptide (rabbit polyclonal, 1:1000 [Millipore, catalog ABS31]), or anti-CD3ζ (mouse monoclonal, 1:1000 [Santa Cruz Biotechnology, clone 6B10.2]) at 4°C for 16 hours. Membranes were washed 3 times for 15 minutes and incubated with a 1:10,000 dilution of HRP-conjugated anti–mouse IgG or anti–rabbit IgG (Thermo Fisher Scientific) for 1 hour. The membranes were washed with TBST 5 times and developed with the SuperSignal West Femto ECL reagents (Thermo Fisher Scientific).

Flow cytometry cytotoxicity assay. Cytotoxic potential of CD19-CAR and CD19-DARIC T cells was analyzed by coincubating T cells with 50:50 mixtures of K562.BFP ($CD19^-$) and Nalm-6.GFP ($CD19^+$) target cells (with or without 1 nM rapamycin or 20 nM AP21967) for 24 hours at an effector to target (Nalm-6) ratio (E/T) of 1:1. The relative percentage of Nalm-6.GFP following T cell coculture was used to calculated the percentage specific T cell cytotoxicity: percentage specific cytotoxicity = $(\%\text{Nalm-6.GFP}^{\text{UTD}} - \%\text{Nalm-6.GFP}^{\text{CD19-CAR or -DARIC}})/\%\text{Nalm-6.GFP}^{\text{UTD}} \times 100$.

All analysis was performed on Attune NxT and the data analyzed using FlowJo and GraphPad Prism.

Incucyte cytotoxicity assay. For live cell imaging, 5×10^3 CD19-CAR or CD19-DARIC T cells were cocultured with 1×10^4 A549-NucRed-CD19 cells or A549-NucGreen-BCMA control cells (E/T ratio at 1:2) with or without rapamycin (1 nM) or AP21967 (20 nM) in the IncuCyte S3 (Essen Bioscience) for 4–6 days. The live target cells were counted via red or green object counts at indicated time points and data analyzed using IncuCyte software and GraphPad Prism.

Click-iT EdU T cell proliferation. For proliferation analysis, CD19-CAR or CD19-DARIC T cells T cells (0.2×10^6 cells) were cocultured with Nalm-6.GFP cells for 3 days (E/T ratio at 1:1) with or without rapamycin (1 nM) or AP21967 (20 nM) in 200 μl TCGM without IL-2. T cell proliferation was evaluated by using the Click-iT Plus EdU Alexa Fluor 594 flow cytometry assay kit (Thermo Fisher Scientific) according to the manufacturer's instructions. Briefly, EdU (4 μM final concentration) was added to the culture for 16 hours. Cells were harvested and stained with anti–human CD3 Alex Fluor 647 (Biolegend). T cells were fixed with 40 μl fixative buffer (component D) for 15 minutes. Washed T cells were then permeabilized in 25 μl 1× Click-iT saponin-based permeabilization and wash reagent for 10 minutes at room temperature. Click-iT reaction mix (125 μl, prepared according to the manufacturer's manual) was added to each sample and incubated in the dark for 30 minutes. Cells were washed and resuspended in 120 μl permeabilization and wash reagent. EdU incorporation in T cells was analyzed by flow cytometry.

Cytokine production analysis. For cytokine secretion analysis, 0.5 × 10^6 T cells were cocultured with Nalm-6.GFP cells (E/T ratio at 1:1) for 24 hours with or without rapamycin (1 nM) or AP21967 (20 nM). Culture supernatants were collected for cytokine (IFN-γ and TNF-α) detection using the Qbeads Plex-Screen kit and analyzed by the iQue Screener (Intellicyt).

DARIC plug-in protein production. A 293T cell line producing the CD19-DARIC plug-in was generated by transducing 293T cells with a lentiviral vector encoding a human CD19-specific scFv fused to FKPB12 followed by a T2A-mCherry reporter transgene. The transduced cells were sorted for mCherry expression using a FACSAriaII cell sorter (BD Biosciences). To purify recombinant CD19-DARIC plug-in, 500 ml 293T cell culture supernatants were collected and filtered (0.22 μm). An FKBP12-specific affinity column was generated by incubating 2 ml NeutrAvidin Agarose (Thermo Fisher Scientific) with 400 μg biotin-FK506 (53) (LifeTein) for 30 minutes at room temperature with constant rotation. The column was washed with PBS to remove uncoupled biotin-FK506. Filtered 293T supernatants were applied to the column by gravity. The column was washed with PBS until absorbance at 280 nm of the flow through was 0. CD19-DARIC plug-in molecules were eluted with 5 ml of 8 μM rapamycin followed by 15 ml PBS. Eluted proteins were concentrated using a VivaSpin-20 centrifugal concentrator (10 kDa MWCO) (Millipore) and washed with PBS using a Zeba Spin 7K column (Thermo Fisher Scientific) to remove residual unbound rapamycin. The purified protein solution was filtered (0.22 μm), sterilized, and stored at 4°C. Because of the high affinity between rapamycin and FKBP12 (Kd = 0.2 nM), the purified CD19-DARIC plug-in is stably bound to rapamycin (Rapa-ready CD19-DARIC plug-in). SDS-PAGE and Western blot analysis using rabbit anti-FKBP12 antibodies confirmed that the purified protein fraction contained a major protein product with molecular weight of approximately 40 kDa without detectable lower-molecular-weight degradation fragments.

Recombinant protein production for rabbit immunization. The CD19-DARIC extracellular domain (FMC63scFv-FKBP12) and FRB were codon optimized for human expression (IDT) and subcloned by Gibson assembly onto the N-terminus of rabbit IgG or human IgG1 Fc CH2-CH3, respectively (pfuse-rIgG-Fc, pINFUSE; Invivogen). Clones were validated by Sanger sequencing and transfection-grade endotoxin-free plasmid was prepared and 0.2-μm filter sterilized in endotoxin-free TE buffer (Qiagen). Protein production was done by transient transfection of Expi293 cells (Thermo Fisher Scientific) using the manufacturer's recommendations. Briefly, on the day of transfection, cells were seeded at approximately 2.5 × 10^6/ml (>95% viability) in fresh Expi293 media and grown for approximately 4–6 hours. Plasmid DNA was diluted to 1 μg/ml in OptiMEM-I and PEI (40K, 1 mg/ml, Polyplus) was diluted at a ratio of 1:2.5 (DNA/PEI) in OptiMEM-I. After a 5-minute incubation, diluted DNA and PEI were combined and incubated for an additional 10–15 minutes before adding drop-wise to cells. Transfected cultures were maintained in 1.6-liter Thomson shake flasks at 800 ml final volume for 5–7 days at 37°C, 8% CO_2, and 150 rpm.

For protein purification, cells and debris were pelleted by centrifugation and supernatant was diluted in binding buffer to final concentration in 20 mM sodium phosphate, pH 7.2, 150 mM NaCl, followed by 0.2-μm filtration. Fc-tagged proteins were affinity purified on the Akta Explorer-100 FPLC using 5-ml HiTrap Protein-A columns (GE Life Sciences), eluted in 0.1 M L-Arg-HCl (pH 3.5), immediately neutralized with 1 M Tris-Cl (pH 8), concentrated to greater than 1 mg/ml (Vivaspin 20, 30, or 50 kDa MWCO), and buffer exchanged to 5% glycerol/PBS (pH 7.4). Monomeric Fc-tagged proteins were further enriched from higher-order aggregates by preparative size-exclusion chromatography using a HiLoad 16/600 Superdex 200 pg column (GE Life Sciences). The desired fractions were pooled, concentrated to 1 mg/ml, 0.2-μm filter sterilized, and analyzed for purity by SDS-PAGE.

Polyclonal antibody generation. In order to recapitulate the recombinant CD19-DARIC complex antigen, equimolar FMC63scFv-FKBP12-rbFc and FRB-rbFc were prepared in sterile 5% glycerol/PBS (pH 7.4) to a final concentration of 1 mg/ml total protein supplemented with 5 μmol rapamycin. Injection material was transferred to R&R Research, LLC and rabbits were immunized according to standard operating protocols.

Rabbit serum was screened for reactivity against the DARIC complex and the individual components by indirect ELISA. Human IgG1-Fc–tagged CD19-DARIC, FKBP12, and FRB were coated at 100 ng/well in 96-well high-protein-binding plates (Corning) and incubated overnight at 4°C. Plates were briefly washed in PBS/Tween (PBST) and blocked with 300 μl/well 1× ELISA/ELISPOT diluent (Thermo Fisher Scientific) for 1–2 hours. A 12-point 2.5-fold serial dilution of serum prebleed or test bleed were performed in 1× diluent and 100 μl was dispensed per well and incubated for 1 hour. After a brief wash in PBST, wells were incubated with a 1:10,000 dilution of goat anti-rabbit HRP (Jackson ImmunoResearch) in 1× diluent for 30 minutes. Plates were again washed with PBST and 100 μl/well 1-Step Ultra TMB (Thermo Fisher Scientific) was added.

After development, reactions were stopped with 100 μl/well of 1N H_2SO_4 and absorbance at 450 nm was measured on a SpectraMax plate reader (Molecular Devices).

Generation of K562 cells expressing various levels of CD19 using mRNA electroporation. The CD19 antigen was PCR amplified from a synthetic gBlock (IDT) using CD19-T7 FP (GGATCCTAATACGACTCACTATAGGGGCCGCCACCATGCCACCTCCTCGCCTCCTCTT) and CD19-RP (CTATTAGCGAGTGCTCCAGGTGCCCATGCGGCCC). PCR product was purified with the QIAquick PCR purification kit (Qiagen), the mRNA was synthesized and polyadenylated with the HiScribe T7 ARCA mRNA in vitro transcription kit (New England Biolabs), and the mRNA purified with the RNeasy mRNA purification kit (Qiagen) following the manufacturer's instructions. The K562 cells were electroporated with indicated amounts of CD19 mRNA using the Neon electroporation system (Thermo Fisher Scientific) using previously described electroporation parameters (54). The electroporated cells were cultured overnight in standard tissue culture conditions and CD19 expression was analyzed by flow cytometry. The cells were counted and used in an AP21967 cytokine coculture assay as described above.

In vivo mouse xenograft studies. Female 6- to 10-week-old NOD.Cg-*Prkdc*^{scid}IL2rg^{tm1Wjl}/SzJ (NSG) mice purchased from Jackson Laboratories were maintained in the bluebird bio vivarium. All studies were conducted according to a study protocol approved by the bluebird bio Institutional Animal Care and Use Committee. Nalm-6 cells stably expressing firefly luciferase (Nalm-6–FFluc) were used to establish the xenograft model. In all studies, the activity of the CD19-CAR or CD19-DARIC T cells was evaluated by determining the tumor size twice weekly using the IVIS Spectrum in vivo imaging system. General safety was evaluated by observing the animals daily and recording their body weights twice weekly. All study personnel were blinded to the identity of the test and control articles. The detailed in vivo experiment setup is described in the Results section.

Statistics. Data analysis was performed using GraphPad Prism 7.0, with significance levels described in specific figure legends. A 2-tailed unpaired Student's *t* test was used for statistical comparison of 2 individual groups. A 1-way ANOVA with Dunnett's test was used for multiparameter statistical comparisons. All figures are presented as mean ± SD.

Study approval. Mouse experiments were performed in Cambridge, Massachusetts, and approved by the bluebird bio IACUC. All mice were monitored for survival, weight loss, and excessive tumor burden, and euthanized according to the IACUC guidelines. All human PBMC lots were purchased from Key Biologics and obtained under an IRB-approved protocol.

Author contributions

AA, JJ, MTC, and WHL conceived and designed the DARIC system. WHL, JG, and UM conducted the in vitro experiments. TEG and HMH performed the in vivo experiments. BRB, RAM, and PDG helped with study design, analysis, and manuscript editing. WHL, JJ, and AA wrote the manuscript.

Acknowledgments

This study was funded and supported by bluebird bio. The authors want to acknowledge Tejeet Banwait and Seema Shah for help with in vivo work, Dong Xia for help with InCyte experiments, and Iva Ivanovska Holder for editing contributions and all the members of the bluebird bio Horizon and Immunotherapy groups for helpful discussions.

1. Gross G, Eshhar Z. Therapeutic potential of T cell chimeric antigen receptors (CARs) in cancer treatment: counteracting off-tumor toxicities for safe CAR T cell therapy. *Annu Rev Pharmacol Toxicol*. 2016;56:59–83.
2. June CH, O'Connor RS, Kawalekar OU, Ghassemi S, Milone MC. CAR T cell immunotherapy for human cancer. *Science*. 2018;359(6382):1361–1365.
3. Maude SL, et al. Tisagenlecleucel in children and young adults with B-cell lymphoblastic leukemia. *N Engl J Med*. 2018;378(5):439–448.
4. Schuster SJ, et al. Chimeric antigen receptor T cells in refractory B-cell lymphomas. *N Engl J Med*. 2017;377(26):2545–2554.
5. Park JH, et al. Long-term follow-up of CD19 CAR therapy in acute lymphoblastic leukemia. *N Engl J Med*. 2018;378(5):449–459.
6. Neelapu SS, et al. Axicabtagene ciloleucel CAR T-cell therapy in refractory large B-cell lymphoma. *N Engl J Med*. 2017;377(26):2531–2544.
7. Mirzaei HR, Rodriguez A, Shepphird J, Brown CE, Badie B. Chimeric antigen receptors T cell therapy in solid tumor: challenges and clinical applications. *Front Immunol*. 2017;8:1850.
8. Srivastava S, Riddell SR. Chimeric antigen receptor T cell therapy: challenges to bench-to-bedside efficacy. *J Immunol*. 2018;200(2):459–468.
9. Gust J, et al. Endothelial activation and blood-brain barrier disruption in neurotoxicity after adoptive immunotherapy with

CD19 CAR-T cells. *Cancer Discov*. 2017;7(12):1404–1419.
10. Hill JA, et al. Infectious complications of CD19-targeted chimeric antigen receptor-modified T-cell immunotherapy. *Blood*. 2018;131(1):121–130.
11. Shalabi H, et al. Sequential loss of tumor surface antigens following chimeric antigen receptor T-cell therapies in diffuse large B-cell lymphoma. *Haematologica*. 2018;103(5):e215–e218.
12. Gardner R, et al. Acquisition of a CD19-negative myeloid phenotype allows immune escape of MLL-rearranged B-ALL from CD19 CAR-T-cell therapy. *Blood*. 2016;127(20):2406–2410.
13. Ruella M, Maus MV. Catch me if you can: Leukemia escape after CD19-directed T cell immunotherapies. *Comput Struct Biotechnol J*. 2016;14:357–362.
14. Jacoby E, et al. CD19 CAR immune pressure induces B-precursor acute lymphoblastic leukaemia lineage switch exposing inherent leukaemic plasticity. *Nat Commun*. 2016;7:12320.
15. Mueller KT, et al. Cellular kinetics of CTL019 in relapsed/refractory B-cell acute lymphoblastic leukemia and chronic lymphocytic leukemia. *Blood*. 2017;130(21):2317–2325.
16. Fraietta JA, et al. Determinants of response and resistance to CD19 chimeric antigen receptor (CAR) T cell therapy of chronic lymphocytic leukemia. *Nat Med*. 2018;24(5):563–571.
17. Hashimoto M, et al. CD8 T cell exhaustion in chronic infection and cancer: opportunities for interventions. *Annu Rev Med*. 2018;69:301–318.
18. Wieland D, et al. TCF1. *Nat Commun*. 2017;8:15050.
19. Viaud S, et al. Switchable control over in vivo CAR T expansion, B cell depletion, and induction of memory. *Proc Natl Acad Sci USA*. 2018;115(46):E10898–E10906.
20. Bachmann D, et al. Retargeting of UniCAR T cells with an in vivo synthesized target module directed against CD19 positive tumor cells. *Oncotarget*. 2018;9(7):7487–7500.
21. Ma JS, et al. Versatile strategy for controlling the specificity and activity of engineered T cells. *Proc Natl Acad Sci USA*. 2016;113(4):E450–E458.
22. Wu CY, Roybal KT, Puchner EM, Onuffer J, Lim WA. Remote control of therapeutic T cells through a small molecule-gated chimeric receptor. *Science*. 2015;350(6258):aab4077.
23. Urbanska K, et al. A universal strategy for adoptive immunotherapy of cancer through use of a novel T-cell antigen receptor. *Cancer Res*. 2012;72(7):1844–1852.
24. Cho JH, Collins JJ, Wong WW. Universal chimeric antigen receptors for multiplexed and logical control of T cell responses. *Cell*. 2018;173(6):1426–1438.e11.
25. Motz G, et al. Abstract B105: ACTR707: a novel T-cell therapy for the treatment of relapsed or refractory CD20$^+$ B cell lymphoma in combination with rituximab. *Mol Cancer Ther*. 2018;17(Suppl–1):B105.
26. Bayle JH, Grimley JS, Stankunas K, Gestwicki JE, Wandless TJ, Crabtree GR. Rapamycin analogs with differential binding specificity permit orthogonal control of protein activity. *Chem Biol*. 2006;13(1):99–107.
27. Choi J, Chen J, Schreiber SL, Clardy J. Structure of the FKBP12-rapamycin complex interacting with the binding domain of human FRAP. *Science*. 1996;273(5272):239–242.
28. Liberles SD, Diver ST, Austin DJ, Schreiber SL. Inducible gene expression and protein translocation using nontoxic ligands identified by a mammalian three-hybrid screen. *Proc Natl Acad Sci USA*. 1997;94(15):7825–7830.
29. Long AH, et al. 4-1BB costimulation ameliorates T cell exhaustion induced by tonic signaling of chimeric antigen receptors. *Nat Med*. 2015;21(6):581–590.
30. Kawalekar OU, et al. Distinct signaling of coreceptors regulates specific metabolism pathways and impacts memory development in CAR T cells. *Immunity*. 2016;44(2):380–390.
31. Kim JH, et al. High cleavage efficiency of a 2A peptide derived from porcine teschovirus-1 in human cell lines, zebrafish and mice. *PLoS ONE*. 2011;6(4):e18556.
32. Juillerat A, et al. Design of chimeric antigen receptors with integrated controllable transient functions. *Sci Rep*. 2016;6:18950.
33. Edwards SR, Wandless TJ. The rapamycin-binding domain of the protein kinase mammalian target of rapamycin is a destabilizing domain. *J Biol Chem*. 2007;282(18):13395–13401.
34. Bäckman L, Kreis H, Morales JM, Wilczek H, Taylor R, Burke JT. Sirolimus steady-state trough concentrations are not affected by bolus methylprednisolone therapy in renal allograft recipients. *Br J Clin Pharmacol*. 2002;54(1):65–68.
35. Friedman KM, et al. Effective targeting of multiple B-cell maturation antigen-expressing hematological malignances by anti-B-cell maturation antigen chimeric antigen receptor T cells. *Hum Gene Ther*. 2018;29(5):585–601.
36. Yatscoff RW, Wang P, Chan K, Hicks D, Zimmerman J. Rapamycin: distribution, pharmacokinetics, and therapeutic range investigations. *Ther Drug Monit*. 1995;17(6):666–671.
37. Saunders RN, Metcalfe MS, Nicholson ML. Rapamycin in transplantation: a review of the evidence. *Kidney Int*. 2001;59(1):3–16.
38. Foster AE, et al. Regulated expansion and survival of chimeric antigen receptor-modified T cells using small molecule-dependent inducible MyD88/CD40. *Mol Ther*. 2017;25(9):2176–2188.
39. Banaszynski LA, Liu CW, Wandless TJ. Characterization of the FKBP.rapamycin.FRB ternary complex. *J Am Chem Soc*. 2005;127(13):4715–4721.
40. Rodgers DT, et al. Switch-mediated activation and retargeting of CAR-T cells for B-cell malignancies. *Proc Natl Acad Sci USA*. 2016;113(4):E459–E468.
41. Lee YG, et al. Use of a single CAR T cell and several bispecific adapters facilitates eradication of multiple antigenically different solid tumors. *Cancer Res*. 2019;79(2):387–396.
42. Law BK. Rapamycin: an anti-cancer immunosuppressant? *Crit Rev Oncol Hematol*. 2005;56(1):47–60.
43. Arriola Apelo SI, et al. Alternative rapamycin treatment regimens mitigate the impact of rapamycin on glucose homeostasis and the immune system. *Aging Cell*. 2016;15(1):28–38.
44. Thomson AW, Turnquist HR, Raimondi G. Immunoregulatory functions of mTOR inhibition. *Nat Rev Immunol*. 2009;9(5):324–337.
45. Pollizzi KN, Powell JD. Regulation of T cells by mTOR: the known knowns and the known unknowns. *Trends Immunol*. 2015;36(1):13–20.

46. Ferrer IR, Araki K, Ford ML. Paradoxical aspects of rapamycin immunobiology in transplantation. *Am J Transplant*. 2011;11(4):654–659.
47. Mannick JB, et al. TORC1 inhibition enhances immune function and reduces infections in the elderly. *Sci Transl Med*. 2018;10(449):eaaq1564.
48. Wherry EJ, Kurachi M. Molecular and cellular insights into T cell exhaustion. *Nat Rev Immunol*. 2015;15(8):486–499.
49. Youngblood B, et al. Effector CD8 T cells dedifferentiate into long-lived memory cells. *Nature*. 2017;552(7685):404–409.
50. Kasakovski D, Xu L, Li Y. T cell senescence and CAR-T cell exhaustion in hematological malignancies. *J Hematol Oncol*. 2018;11(1):91.
51. Kang CB, Hong Y, Dhe-Paganon S, Yoon HS. FKBP family proteins: immunophilins with versatile biological functions. *Neurosignals*. 2008;16(4):318–325.
52. Milone MC, et al. Chimeric receptors containing CD137 signal transduction domains mediate enhanced survival of T cells and increased antileukemic efficacy in vivo. *Mol Ther*. 2009;17(8):1453–1464.
53. McPherson M, Yang Y, Hammond PW, Kreider BL. Drug receptor identification from multiple tissues using cellular-derived mRNA display libraries. *Chem Biol*. 2002;9(6):691–698.
54. Sather BD, et al. Efficient modification of CCR5 in primary human hematopoietic cells using a megaTAL nuclease and AAV donor template. *Sci Transl Med*. 2015;7(307):307ra156.